The inhibition of gadolinium ion (Gd^{3+}) on the mitochondrial F$_1$F$_O$-ATPase is linked to the modulation of the mitochondrial permeability transition pore

Cristina Algieri, Fabiana Trombetti, Alessandra Pagliarani*, Micaela Fabbri, Salvatore Nesci*

Department of Veterinary Medical Sciences (DIMEVET), University of Bologna, via Tolara di Sopra, 50, 40064 Ozzano Emilia (Bologna), Italy.

*Corresponding authors: alessandra.paliarani@unibo.it (AP); salvatore.nesci@unibo.it (SN)

Keywords: gadolinium ion; mitochondria; F$_1$F$_O$-ATPase; permeability transition pore; metal cofactors; enzyme kinetics.

Abstract

The mitochondrial permeability transition pore (PTP), which drives regulated cell death when Ca^{2+} concentration suddenly increases in mitochondria, was related to changes in the Ca^{2+}-activated F_1F_O-ATPase. The effects of the gadolinium cation (Gd^{3+}), widely used for diagnosis and therapy, and reported as PTP blocker, were evaluated on the F_1F_O-ATPase activated by Mg^{2+} or Ca^{2+} and on the PTP. Gd^{3+} more effectively inhibits the Ca^{2+}-activated F_1F_O-ATPase than the Mg^{2+}-activated F_1F_O-ATPase by a mixed-type inhibition on the former and by uncompetitive mechanism on the latter. Most likely Gd^{3+} binding to F_1, is favoured by Ca^{2+} insertion. The maximal inactivation rates (K_{inact}) of pseudo-first order inactivation are similar either when the F_1F_O-ATPase is activated by Ca^{2+} or by Mg^{2+}. The half-maximal inactivator concentrations (K_I) are 2.35 ± 0.35 mM and 0.72 ± 0.11 mM, respectively. The potency of a mechanism-based inhibitor (K_{inact}/K_I) also highlights a higher inhibition efficiency of Gd^{3+} on the Ca^{2+}-activated F_1F_O-ATPase (0.59 ± 0.09 $mM^{-1} \cdot s^{-1}$) than on the Mg^{2+}-activated F_1F_O-ATPase (0.13 ± 0.02 $mM^{-1} \cdot s^{-1}$). Consistently, the PTP is desensitized in presence of Gd^{3+}. The Gd^{3+} inhibition on both the mitochondrial Ca^{2+}-activated F_1F_O-ATPase and the PTP strengthens the link between the PTP and the F_1F_O-ATPase when activated by Ca^{2+} and provides insights on the biological effects of Gd^{3+}.

2

1. Introduction

The F_1F_O-ATPase, an oligomeric complex of the inner mitochondrial membrane (IMM) ubiquitous in mammals, is an energy-transducing machine characterized by a reversible working mode of ATP synthesis/hydrolysis [1]. According to the chemiosmotic theory, the H^+ transfer from the mitochondrial matrix to the intermembrane space by the respiratory complexes, pushed by substrate oxidation, creates the protonmotive force (Δp) that is converted into a useful chemical form, ATP [2]. Contrary, in the reverse-mode, the hydrolysis of the high-energy phosphoanhydridic bonds of ATP drives H^+ pumping in the intermembrane space and energizes the IMM. The bi-functional catalysis of the F_1F_O-ATPase is a unique energy transmission mechanism sustained by the structural enzyme arrangement in two molecular motors, a hydrolytic F_1 sector and a hydrophobic F_O sector. The two sectors are coupled by a reversible torque generation [3,4] (Fig. 1). The catalytic domain F_1 is a globular hexamer in which three α subunits and three β subunits alternate. F_1 contains three catalytic and three non-catalytic sites which bind adenine nucleotides. The catalytic sites are each β subunit at the interface with the adjacent α subunit, whereas the non-catalytic sites are on each α subunit at the interface with the adjacent β subunit [5]. During the ATP synthesis/hydrolysis, according to the "binding change model" [6], the conformational change in the $(\alpha\beta)_3$ assembly occurs during the rotor rotation. During a 360° rotation the catalytic and non-catalytic site conformations change in TP (binding ATP), DP (binding ADP), and E (empty) conformations, driven by the rotation of the central stalk. The β subunits undergo a decrease in affinity for nucleotides with the sequential transition $\beta_{TP} \rightarrow \beta_{DP} \rightarrow \beta_E$, while the α subunits only undergo the conformational changes during the rotor rotation. This mechanochemical mechanism of the F_1 domain is driven by the H^+ flow through F_O which generates the torsional movement. The H^+ translocation from one side to the opposite side of the IMM within two asymmetrical half-channels on *a* subunit at the interface with the *c*-ring which hosts the H^+ binding sites [7]. Differently from the bacterial enzyme, the mitochondrial F_O domain contains supernumerary subunits which intervene during the enzyme dimerization and oligomerization, which in turn play a morphological role in mitochondrial *crista* formation [8,9]. Moreover, the supernumerary subunits are important to form and open the permeability transition pore (PTP) inside the *c*-ring [10].

Accordingly, the IMM becomes permeable to solutes up to 1.5 kDa in a process defined permeability transition (PT) when the PTP, a Ca^{2+}-activated channel with high conductance, opens. It seems ascertained that the F_1F_O-ATPase is the main playmaker which triggers the PTP formation and opening. Additionally, a low conductance channel inhibited by both CsA and BKA could be formed by the adenine nucleotide translocase isoforms [11,12]. After about 50 years of debate, the arcane molecular mechanism of PTP was revealed by Sazanov's group [10]. When Ca^{2+} concentration increases in the mitochondrial matrix, the F_1F_O-ATPase can replace the natural cofactor Mg^{2+} with Ca^{2+} on β subunits [13]. The Ca^{2+}-activated enzyme can sustain ATP hydrolysis [14]. Since Ca^{2+} has a larger atomic radius than Mg^{2+} it induces conformational changes in the F_1 domain which are transmitted to the membrane-embedded subunits [15]. Under physiological and pathological conditions, according to the "bent-pull" model of the Ca^{2+}-activated F_1F_O-ATPase [16], the PTP opens within the *c*-ring. In detail, the lipid plug anchored to *e* subunit, a lyso-phosphatidylserine which penetrates and fills the hole of the *c*-ring at the intermembrane space, is pulled out by *e* subunit displacement. The different conformational states of the F_1F_O-ATPase when activated by Ca^{2+}, which apparently cannot occur when Mg^{2+} plays the cofactor role, permit the detachment of the F_1 domain by pushing the phosphatidylserine that fills the hole at the matrix side when water molecules enter the *c*-ring [10]. The F_1F_O-ATPase activated by Ca^{2+} as cofactor undergoes conformational changes which open the PTP [17]. Since PTP opening leads to cell death [18] and PTP dysregulation is increasingly involved in severe human diseases [2], once identified the main macromolecular target responsible for PTP formation, several compounds have been considered and investigated as potential pore inhibitors [19].

The rare earth transition metals known as Lanthanides are widely used in medicine due to their physicochemical characteristics [20]. They play an increasingly recognized role in diagnosis and therapy,

other than being widely exploited in research. Gadolinium (Gd)-based compounds belonging to organometals are widely used in Magnetic Resonance Imaging (MRI) as a contrast medium [21] as well as putative anticancer drugs [22]. Although for clinical use Gd ion (Gd^{3+}) is always chelated with specific ligands due to its high toxicity, it seems to accumulate in the tissues, especially in the brain, therefore its long-term use has raised emerging concern [23]. Interestingly, the trivalent Gd^{3+} has biophysical characteristics similar to the divalent Ca^{2+} (radius of Gd^{3+} 1.05-1.11 Å vs Ca^{2+} 1.00-1.06 Å), which allow it to replace Ca^{2+} in its biological and biochemical mechanisms. Accordingly, the biological effects are currently ascribed to the cationic form Gd^{3+}. Most likely, Gd^{3+} acts at the cellular level by directly interfering with the Ca^{2+} entry pathways. Gd^{3+} is also used in experimental tests as an inhibitor of Ca^{2+} channels activated by stretching [24]. The Gd^{3+}-based compounds used in MRI seem to have negative effects on the mitochondrial activity by altering ATP production, reducing mitochondrial oxidative capacities and also promoting cellular apoptosis [25] and other forms of cell death [26]. These effects were also related to the Gd^{3+} capability to promote PTP opening [27]. Conversely, the cation was also reported to act as a PTP blocker in mammalian mitochondria [16].

The possibility that Gd^{3+} may act on the mammalian F_1F_O-ATPase activated by Ca^{2+} differently from the Mg^{2+}-activated enzyme was investigated and compared with the effects on PTP opening. The results may not only contribute to casting light on some still unexplored molecular mechanisms of Gd^{3+} toxicity [26], but also may improve the knowledge on the mechanism of PTP formation and opening and broaden the spectrum of exogenous PTP modulators. Moreover, since membrane permeabilization often results in a cellular catastrophe and Gd^{3+} is widely employed in medical fields, such as research, diagnosis and therapy, the assessment of the Gd^{3+} action mechanism on the key enzyme in bioenergetics may be extremely useful to adequately exploit Gd^{3+} properties for medical purposes.

2. Materials and methods

2.1. Chemicals

Oligomycin (a mixture of oligomycins A, B and C), and Fura-FF were purchased from Vinci-Biochem (Vinci, Italy). Na_2ATP and gadolinium trichloride ($GdCl_3$) were obtained from Sigma–Aldrich (Milan, Italy). Quartz double distilled water was used for all reagent solutions.

2.2. Preparation of the mitochondrial fractions

Swine hearts (*Sus scrofa domesticus*) were collected at a local abattoir and transported to the lab within 2 h in ice buckets at 0–4°C. After removal of fat and blood clots as much as possible, approximately 30–40 g of heart tissue was rinsed in ice-cold washing Tris-HCl buffer (medium A) consisting of 0.25 M sucrose, 10 mM Tris(hydroxymethyl)-aminomethane (Tris), pH 7.4 and finely chopped into fine pieces with scissors. Each preparation was made from one heart. Once rinsed, tissues were gently dried on blotting paper and weighted. Then tissues were homogenized in medium B consisting of 0.25 M sucrose, 10 mM Tris, 1 mM EDTA (free acid), 0.5 mg/ml BSA fatty acid free, pH 7.4 with HCl at a ratio of 10 ml medium B per 1 g of fresh tissue. After a preliminary gentle break up by Ultraturrax T25, the tissue was carefully homogenized by a motor-driven teflon pestle homogenizer (Braun Melsungen Type 853202) at 650 rpm with 3 up-and-down strokes. The mitochondrial fraction was then obtained by stepwise centrifugation (Sorvall RC2-B, rotor SS34). Briefly, the homogenate was centrifuged at 1,000x*g* for 5 min, thus yielding a supernatant and a pellet. The pellet was re-homogenized under the same conditions of the first homogenization and re-centrifuged at

1,000x*g* for 5 min. The gathered supernatants from these two centrifugations, filtered through four cotton gauze layers, were centrifuged at 10,500x*g* for 10 min to yield the raw mitochondrial pellet. The raw pellet was resuspended in medium A and further centrifuged at 10,500x*g* for 10 min to obtain the final mitochondrial pellet. The latter was resuspended by gentle stirring using a Teflon Potter Elvejehm homogenizer in a small volume of medium A, thus obtaining a protein concentration of 30 mg/ml [28]. All steps were carried out at 0–4°C. The protein concentration was determined according to the colorimetric method of Bradford [29] by Bio-Rad Protein Assay kit II with BSA as standard. The mitochondrial preparations were then stored in liquid nitrogen until the evaluation of F_1F_O-ATPase activities.

2.3. Mitochondrial F-ATPase activity assays

Thawed mitochondrial preparations were immediately used for F-ATPase activity assays. The capability of ATP hydrolysis was assayed in a reaction medium (1 ml). The optimal conditions to obtain the maximal activity of the F_1F_O-ATPase, which depend on substrates concentration and pH values, are at 0.15 mg mitochondrial protein and 75 mM ethanolammine–HCl buffer pH 9.0, 6.0 mM Na_2ATP and 2.0 mM $MgCl_2$ for the Mg^{2+}-activated F_1F_O-ATPase assay, and 75 mM ethanolammine–HCl buffer pH 8.8, 3.0 mM Na_2ATP and 2.0 mM $CaCl_2$ for the Ca^{2+}-activated F_1F_O-ATPase assay [14,30]. These assay conditions were previously proven to elicit the maximal enzyme activities either stimulated by Mg^{2+} or by Ca^{2+} in swine heart mitochondria [31]. After 5 min preincubation at 37°C, the reaction, carried out at the same temperature, was started by the addition of the substrate Na_2ATP and stopped after 5 min by the addition of 1 ml of ice-cold 15% (w/w) trichloroacetic acid (TCA) aqueous solution. Once the reaction was stopped, vials were centrifuged for 15 min at 3,500 rpm (Eppendorf Centrifuge 5202). In the supernatant, the concentration of inorganic phosphate (Pi) hydrolyzed by known amounts of mitochondrial protein, which is an indirect measure of F-ATPase activity, was spectrophotometrically evaluated [32]. According to the method employed, to detect the Pi release by the enzymatic reaction, the Pi released independently of the F_1F_O-ATPase activity should be quantified. To this aim, 1 μl from a stock solution of 3 mg/ml oligomycin in dimethylsulfoxide was directly added to the reaction mixture before starting the reaction. The total ATPase activity was calculated by detecting the Pi in control tubes run in parallel and containing 1 μl dimethylsulfoxide per ml reaction system. In each experimental set, control tubes were alternated to the condition to be tested. The employed dose of oligomycin, specific inhibitor of F-ATPases which selectively blocks the F_O subunit ensured maximal enzyme activity inhibition and was currently used in F-ATPase assays [30].

To test the effect of Gd^{3+} on the differently activated F_1F_O-ATPase activities, aqueous solutions of $GdCl_3$ at different standard concentrations were prepared immediately before each experimental set. Small aliquots (10 μl) of these solutions were added to the reaction system and incubated at 37°C before starting the F_1F_O-ATPase reaction. Control tubes contained the same final volume, adjusted with 10 μl of the reaction buffer.

In all experiments, the F_1F_O-ATPase activity was routinely measured by subtracting, from the Pi hydrolyzed by total ATPase activity, the Pi hydrolyzed in the presence of oligomycin [28]. In all experiments the F-ATPase activity, either activated by Ca^{2+} as cofactor or by Mg^{2+}, was expressed as μmol Pi·mg protein^{-1}·min^{-1}.

2.4. Kinetic analyses

The inhibition mechanism of Gd^{3+} on the Ca^{2+}- or Mg^{2+}-activated F_1F_O-ATPases was explored by the graphical methods of Dixon and Cornish-Bowden plots, which complement one another. [33] To this aim, the 1/*v* (reciprocal of the enzyme activity *v*) in Dixon plot or the S/*v* ratio in Cornish-Bowden plot were plotted as a

function of GdCl$_3$ concentration. In all plots the enzyme specific activity was taken as the expression of *v*. To build these plots, different experimental sets were designed in which the F-ATPase activity was evaluated in the presence of increasing GdCl$_3$ concentrations at two ATP concentrations, keeping the divalent cofactor (Mg^{2+} or Ca^{2+}) concentration constant. In these plots and in the definition of the binary or ternary complexes *S* indicates the ATP substrate. The values of K$_i$, which corresponds to the dissociation constant of the *EI* complex were calculated from the abscissa (changed to positive) of the intercept of the straight lines obtained in the Dixon plots. The values of K'$_i$, which represent the dissociation constant of the ternary *ESI* complex, were calculated as the abscissa (changed to positive) of the intercept of the straight lines obtained in the Cornish-Bowden plots.

The inactivation kinetics was investigated by incubating the mitochondrial suspensions in the presence of various GdCl$_3$ concentrations (1.0 – 2.0 – 4.0 mM GdCl$_3$ when the F$_1$F$_O$-ATPase was activated by Mg^{2+} as cofactor, and 1.0 – 1.5 – 2.0 mM GdCl$_3$ when the F$_1$F$_O$-ATPase was activated by Ca^{2+}). The F$_1$F$_O$-ATPase reaction activated by either Mg^{2+} or Ca^{2+} as cofactor was stopped after different time intervals (1-7 min) by 1 ml TCA 15% (w/w) addition. The pseudo first-order rate constants (k_{obs}) for the enzyme inactivation were determined in both cases by plotting the natural logarithm of the residual activity *vs* time and extracting the rate constant from the slope [34].

A double-reciprocal plot is created by plotting the $1/k_{obs}$ (*x* axis) as a function of the inverse of the GdCl$_3$ concentrations (1/[GdCl$_3$]) (*y* axis). The maximal inactivation rate (k_{inact}) can be accurately determined and thus the inhibitor concentration at ½k_{inact} (K$_I$) can also be determined with accuracy because a straight line is formed. The *y*-intercept is $1/k_{inact}$, and the *x*-intercept is -1/K$_I$. The ratio k_{inact}/K$_I$ is used to calculate the inhibitor efficiency, a rate constant for the potency of a mechanism-based inhibitor [35].

2.5. Evaluation of PTP

Immediately after the preparation of swine heart mitochondrial fractions, fresh mitochondrial suspensions (1mg/ml) were energized in the assay buffer (130 mM KCl, 1 mM KH$_2$PO$_4$, 20 mM HEPES, pH 7.2 with TRIS), incubated at 25°C with 1 µg/ml rotenone and 5 mM succinate as respiratory substrate. To evaluate Gd^{3+} effect, selected Gd^{3+} concentrations, obtained by sampling small aliquots from standard GdCl$_3$ aqueous solutions, as described in Section 2.3, were added to the mitochondrial suspensions before PTP evaluation. PTP opening was induced by the addition of low concentrations of Ca^{2+} (10 µM) as CaCl$_2$ aqueous solution at fixed time intervals (1 min). The Ca^{2+} retention capacity (CRC), whose lowering indicates mPTP opening, was spectrofluorophotometrically evaluated in the presence of 0.8 µM Fura-FF. The probe has different spectral properties in the absence and in the presence of Ca^{2+}, namely it displays excitation/emission spectra of 365/514 nm in the absence of Ca^{2+} (Fura-FF low Ca^{2+}) and shifts to 339/507 nm in the presence of high Ca^{2+} concentrations (Fura-FF high Ca^{2+}). PTP opening, was evaluated by the increase in the fluorescence intensity ratio (Fura-FF high Ca^{2+})/(Fura-FF low Ca^{2+}), which indicates a decrease in CRC [36]. All measurements were processed by LabSolutions RF software.

2.6. Calculations and statistics

The data represent the mean ± SD (shown as vertical bars in the figures) of the number of experiments reported in the figure captions. In each experimental set, the analyses were carried out on different pools of animals. Statistical analyses were performed by SIGMASTAT software. The analysis of variance followed by Students–Newman–Keuls' test when F values indicated significance ($P \le 0.05$) was applied. Percentage data were *arcsin*-transformed before statistical analyses to ensure normality.

3. Results and discussion

The mPTP opening and the mitochondrial F_1F_O-ATPase participation in the mPTP are both linked to an abrupt Ca^{2+} increase in mitochondria. In detail, the substitution of the natural cofactor Mg^{2+} by Ca^{2+} as cofactor in the β subunits of the F_1F_O-ATPase [13] has been involved in the mechanism of mPTP formation [9,30]. The mitochondrial F_1F_O-ATPase can be activated by either Mg^{2+} or Ca^{2+}, which can both act as cofactor, even if by displaying different kinetic features [14,17]. The rare earth metal cation Gd^{3+}, whose effects on the mPTP are still partially known, offers the opportunity to verify the effect on the F_1F_O-ATPase and to explore its putative connection with the mPTP. Accordingly, Gd^{3+} was reported to induce mitochondrial dysfunction, probably due to PTP opening [27]. Acute toxicity of the intraperitoneally injected salt of all the stable rare earth compounds in mice at level of 300 to 500 mg/Kg were produced [37]. In erythrocyte membranes Gd^{3+}, which is able to interact with membrane phospholipids [38], would act as pore former [39]. Conversely, Gd^{3+} was shown to inhibit membrane permeabilization by physically modifying the membrane structure in a model system [40]. In this paper all the mitochondrial effects of Gd^{3+} were tested by adding selected concentrations of the chloride salt $GdCl_3$ which in aqueous media dissociates yelding Gd^{3+} and Cl^-. We tried to exploit the Gd^{3+} inhibition mechanism to understand its modulatory role of Gd^{3+} on the Ca^{2+}-activated F_1F_O-ATPase when the PTP forms. So the observed effects are currently ascribed to Gd^{3+}, known to interact with proteins.

3.1. Gd^{3+} affects the F_1F_O-ATPase activity either activated by Mg^{2+} or by Ca^{2+}

The effect of $GdCl_3$, in the range of $0.01 - 5.0$ mM, was evaluated on the F_1F_O-ATPase either activated by Mg^{2+} or by Ca^{2+} as cofactor (Fig. 2). Increasing $GdCl_3$ concentrations promotes an exponential F_1F_O-ATPase activity decay independently of the divalent cofactors that sustain ATP hydrolysis. Both the differently activated F_1F_O-ATPase activities are increasingly inhibited by increasing $GdCl_3$ concentrations. However, the main difference between the F_1F_O-ATPase activities when activated by Mg^{2+} or by Ca^{2+} as cofactor is that the F_1F_O-ATPase when activated by Mg^{2+} only attains a maximal 40% inhibition at the highest concentration tested (5mM $GdCl_3$) (Fig. 2A), while when activated by Ca^{2+} the enzyme is progressively inhibited up to attain a value close to zero at 5 mM $GdCl_3$ (Fig. 2B).

3.2. The Inhibition mechanism is revealed by inhibition kinetics analyses

Kinetic studies, based on the building of Dixon and Cornish-Bowden plots, can lead to define the features of the enzyme–inhibitor complex in the presence or in the absence of the ATP substrate or cation cofactors. These kinetic analyses were carried out to understand the $GdCl_3$ inhibition mechanism, most likely exerted by Gd^{3+}, on the F_1F_O-ATPase. The inhibition exerted by Gd^{3+} on the Mg^{2+}-activated F_1F_O-ATPase shows a competitive mechanism with respect to the ATP substrate (Fig. 3A,B) and an uncompetitive type mechanism with respect to the Mg^{2+} cofactor (Fig. 3C,D). The competitive inhibition indicates that the inhibitor only binds to the free enzyme, while the uncompetitive inhibition indicates that Gd^{3+} only binds to the enzyme-Mg^{2+} complex. According to the mechanism of uncompetitive inhibition, usually observed when the enzyme has two or more binding sites [41], Gd^{3+} binds to a different site than that of the Mg^{2+} cofactor, but only when the enzyme–substrate (*ES*) complex is already formed, to yield the enzyme–substrate-inhibitor (*ESI*) complex.

The competitive inhibition mechanism is also exerted by Gd^{3+} on the Ca^{2+}-activated F_1F_O-ATPase with respect to the ATP substrate (Fig. 4A,B). Gd^{3+} blocks the ATP binding to the enzyme by inhibiting the ATPase activity irrespective of the cation cofactor. The K_i value of the F_1F_O-ATPase is about three times lower than that of

the Mg^{2+}-activated F_1F_O-ATPase (0.5±0.4 mM *vs* 1.4±0.1 mM) (Table 1). These K_i values indicate that Gd^{3+} more efficiently competes with ATP in the substrate binding site to form the binary complex (*EI*) when the F_1F_O-ATPase is activated by Ca^{2+} as cofactor than when the enzyme is activated by Mg^{2+}. Moreover, when the natural cofactor Mg^{2+} is substituted by Ca^{2+}, the F_1F_O-ATPase undergoes a mixed type inhibition mechanism on the cofactor (Fig. 4C,D). This inhibition type indicates that the inhibitor Gd^{3+} can bind either to the free enzyme or to the enzyme Ca^{2+}-complex. These results prove that Gd^{3+} and Ca^{2+} bind to distinct enzyme sites. Since the Gd^{3+} binding site does not overlap with the Ca^{2+} binding site on β subunits [13], the Ca^{2+}-activated F_1F_O-ATPase can form either a binary (enzyme-Gd^{3+}) or a ternary (Ca^{2+}-enzyme-Gd^{3+}) complex with the inhibitor. However, on considering the dissociation constants of the enzyme-inhibitor complex (K_i) and of the enzyme-substrate-inhibitor complex (K'_i), since the K_i value is three times lower than the K'_i value, the formation of the binary complex (enzyme-Gd^{3+}) is preferred with respect to that of the ternary complex (enzyme-cofactor-inhibitor). Moreover, the K'_i values in the presence of Mg^{2+} or Ca^{2+} as cofactor are similar (Table 1), thus pointing out that the ternary complex is independent of the activating cation. In other words, even if Gd^{3+} preferentially binds to the enzyme before the cofactor binding to form the binary complex, it binds to the enzyme-cofactor complex to form the ternary complex with the same strength when the cofactor is Mg^{2+} or Ca^{2+}.

3.3. How the cofactor may affect the F_1F_O-ATPase function

The different size of cations with a larger radius than Mg^{2+} (1.45 Å) such as Ca^{2+} (1.94 Å) would promote a different coordination chemistry in the catalytic sites of the F_1 hexamer. The hypothesized more flexible coordination geometry, characterized by irregular bond distances and angles in the β subunits induced by Ca^{2+}, allows the accommodation of up to eight bonds while Mg^{2+} forms hexacoordinated octahedral complexes [42]. The nucleotide-binding to the catalytic and non-catalytic F_1F_O-ATPase subunits requires the coordination of the essential cofactor Mg^{2+} which contributes to yield the binding site asymmetry and generation of the different affinities for nucleotides [43]. The presence of Ca^{2+} as cofactor modifies the enzyme kinetic parameters [14] and ascribes to the F_1F_O-ATPase a new role in mitochondrial biology [9,17]. Indeed, the new cryo-EM structure of the F_1F_O-ATPase [10] highlights a thorough conformational change in the enzyme structure when the Ca^{2+} replaces Mg^{2+} in the catalytic site and triggers the PTP formation according to the "bent-pull" model of the *c*-ring-gated channel [16]. The role of Ca^{2+} in the catalytic sites of the enzyme is corroborated by mutagenesis studies carried out by Bernardi's group [15]. Among the six bonds that coordinate the Mg^{2+} cofactor, only the βThr163 of P-loop is directly linked to the cation. The Thr-Ser substitution promotes a selective decrease in mitochondrial Ca^{2+}-ATPase hydrolysis of ATP [15,44] associated with a resistance to the Ca^{2+}-induced PTP opening [15].

The reduction in the F_1F_O-ATPase catalytic efficiency of upon exposure to Gd^{3+} helps to correlate the enzyme structure and function in a selected domain, and to understand the enzyme involvement in PTP formation. The natural logarithm of the residual activity (uninhibited rate minus inhibited rate) *vs* time provides the observed first-order rate constants calculated from the slopes of the straight lines obtained at different $GdCl_3$ concentrations when either Mg^{2+} or Ca^{2+} act as cofactor of the F_1F_O-ATPase activity. The plots in Figure 5A and 6A show the typical time course of Gd^{3+}-mediated inhibition on the activity of the F_1F_O-ATPase when activated either by Mg^{2+} or by Ca^{2+} as cofactor, respectively. In both cases, the time course of the Gd^{3+}-mediated inhibition is well fitted to an exponential function. The k_{obs}, which is obtained from the slope of each straight line, displays a gradual $GdCl_3$ concentration-dependent increase only when the F_1F_O-ATPase is activated by Mg^{2+} (Fig. 5A). The inhibition mechanism of Gd^{3+} on the Mg^{2+}- or the Ca^{2+}-activated F_1F_O-ATPase, depicted in figure 5B and figure 5B, respectively, shows the $GdCl_3$ concentrations which promote the half-maximal enzyme inactivation in the presence of different cofactors. The F_1F_O-ATPase when activated by Ca^{2+}

as cofactor shows a three times lower K_i value than when it is activated by Mg^{2+}-activated F_1F_O-ATPase (Table 1), suggesting that Gd^{3+} bound to the catalytic region affects the kinetics of cofactor-mediated ATP hydrolysis. The higher propensity of Gd^{3+} to react with the F_1F_O-ATPase when activated by Ca^{2+} than when activated by Mg^{2+} is also confirmed by a significantly higher k_{inact} value for the Ca^{2+}-activated F_1F_O-ATPase (Table 1). The inhibition potency of Gd^{3+}, which indicates the Gd^{3+} inhibition efficiency on the Mg^{2+}- and the Ca^{2+}-activated F_1F_O-ATPase, is shown by the k_{inact}/K_I ratio (Table 1). Gd^{3+} shows a k_{inact}/K_I ratio for the Ca^{2+}-activated F_1F_O-ATPase, which is 4.5 times higher than the ratio for the Mg^{2+}-activated F_1F_O-ATPase (Table 1). Therefore, Gd^{3+} more quickly reacts with the enzyme in the presence of Ca^{2+} as cofactor, resulting in a prompter and stronger inhibition of the F_1F_O-ATPase activity when activated by Ca^{2+} as cofactor. To sum up, all data indicate that when Ca^{2+} replaces the natural cofactor Mg^{2+} in the enzyme binding site, the F_1F_O-ATPase becomes more prone to the inhibition by Gd^{3+}.

3.4. PTP desensitization to Ca^{2+}

Ca^{2+} pulses accumulate in the mitochondrial matrix and are released when the PTP opens. Mitochondria retain calcium and do not form the PTP until the IMM remains intact. The CRC, represents the capability of intact mitochondria to accumulate Ca^{2+}. According to the method adopted, the CRC decrease in $GdCl_3$ treated mitochondria, revealed by an increase in fluorescence intensity, points out the Gd^{3+} ability to desensitize the PTP opening (Fig. 7A). In control mitochondria, the CRC decrease is revealed after 210 sec upon a two-train Ca^{2+} pulses, as shown by the rise in the (Fura-FF high Ca^{2+})/(Fura-FF low Ca^{2+}) ratio. Accordingly, the increase in CRC upon subsequent 10 μM Ca^{2+} additions at 1 min intervals, indicates that mitochondria in the presence of Gd^{3+} must attain a higher threshold value of Ca^{2+} concentration in the matrix to trigger PTP formation, with respect to control mitochondria. This phenomenon, known as PTP desensitization to Ca^{2+}, is shown by a delayed rise in the Fura-FF ratio, which indicates a decreased CRC (Fig. 7A). Consistently, the PTP formation extent, expressed as the ratio of the number of Ca^{2+} pulses required to induce the PTP in MgADP inhibited (CRC_i) and untreated (CRC_o) mitochondria [31], is doubled in the presence of 1.0 mM $GdCl_3$ (Fig. 7B).

3.5. The Gd^{3+} inhibition of the F_1F_O-ATPase activity when Ca^{2+} acts as cofactor is consistent with the PTP desensitization

We can speculate that the $GdCl_3$ effects on the PTP are due to the interactions of Gd^{3+} in the F_1 region of the F_1F_O-ATPase, which hamper the PTP formation. The $GdCl_3$ preferential inhibition on the F_1F_O-ATPase when the cofactor is Ca^{2+} corroborates the link between the Ca^{2+}-activated F_1F_O-ATPase and the PTP and points out Gd^{3+} as a PTP inhibitor, consistently with other reports in swine mitochondria [44]. On the other hand, Lanthanide ions are long known as blockers of membrane permeabilization [40], even if this topic is still controversial [45]. Under the experimental conditions adopted, the strong binding of Gd^{3+} to the F_1F_O-ATPase catalytic domain when the enzyme activity is activated by Ca^{2+} hampers both ATP hydrolysis and PTP formation.

4. Conclusion

The results add further information on the mitochondrial effects of Gd^{3+}, which from a literature overview, are still controversial. Lanthanide ions including Gd^{3+} were shown to increase mitochondrial fluidity and to promote mitochondrial swelling and apoptosis in mice liver, thus strongly suggesting the induction of PTP opening [45]. Gd^{3+} promoted PTP opening in rat liver mitochondria at 500 μM concentration [27] and induced mitochondrial impairment and neuronal cell apoptosis [46]. On the contrary, recently Gd^{3+} was reported as

9

known PTP blocker in mammalian mitochondria [16]. These reports open intriguing questions on the PTP modulation by exogenous compounds. Most likely the Gd^{3+} effect and action mechanism on the membrane permeabilization mainly depend on the dose and on the experimental conditions. The concentration-dependent effects of Gd^{3+} on mitochondria were already pointed out [47].

On these bases, the mitochondrial membrane composition and the Gd^{3+} concentration may be crucial in determining the accessibility of Gd^{3+} to the F_1F_O-ATPase, especially on considering that Gd^{3+} by interacting with membrane phospholipids can modify the membrane structure [45].

The inhibition kinetic analyses confirm that in swine heart mitochondria the F_1F_O-ATPase is a molecular target of Gd^{3+} which directly interacts with the enzyme proteins. The Gd^{3+} effect on the F_1F_O-ATPase catalytic activity reinforces the link between PTP formation and the F_1F_O-ATPase activation in the presence of Ca^{2+} as cofactor. Indeed, Gd^{3+}, not only blocks PTP opening, but exerts a more efficient F_1F_O-ATPase inhibition when the natural Mg^{2+} cofactor is replaced by Ca^{2+}. Assuming that the enzyme has different conformations when it binds Mg^{2+} or Ca^{2+} [10] the molecular model that ascribes to Ca^{2+} insertion in the catalytic F_1F_O-ATPase sites the event which triggers the F_1F_O-ATPase conformational changes which open the PTP [9,15,17] is strongly corroborated. The role of Gd^{3+} as PTP blocker opens new perspectives in the putative protective role of this cation to prevent mitochondrial decay and cell death. Accordingly, $GdCl_3$ administration to counteract ischemia/riperfusion injury was reported to attenuate the mitochondrial damage in liver cells [48] as well as cardiomyocyte apoptosis in rats [49]. Gd^{3+} derivatives inhibited the mitochondrial pathway of apoptosis in human hepatocytes [50]. However, since the mitochondrial effects of Gd^{3+} are still poorly investigated, any extrapolation should be taken with caution and further studies are required.

References

[1]   W. Junge, H. Sielaff, S. Engelbrecht, Torque generation and elastic power transmission in the rotary F(O)F(1)-ATPase, Nature. 459 (2009) 364–370. https://doi.org/10.1038/nature08145.

[2]   S. Nesci, F. Trombetti, A. Pagliarani, V. Ventrella, C. Algieri, G. Tioli, G. Lenaz, Molecular and Supramolecular Structure of the Mitochondrial Oxidative Phosphorylation System: Implications for Pathology, Life. 11 (2021) 242. https://doi.org/10.3390/life11030242.

[3]   W. Kühlbrandt, Structure and Mechanisms of F-Type ATP Synthases, Annu. Rev. Biochem. 88 (2019) 515–549. https://doi.org/10.1146/annurev-biochem-013118-110903.

[4]   S. Nesci, A. Pagliarani, C. Algieri, F. Trombetti, Mitochondrial F-type ATP synthase: multiple enzyme functions revealed by the membrane-embedded FO structure, Crit. Rev. Biochem. Mol. Biol. 55 (2020) 309–321. https://doi.org/10.1080/10409238.2020.1784084.

[5]   A. Hahn, K. Parey, M. Bublitz, D.J. Mills, V. Zickermann, J. Vonck, W. Kühlbrandt, T. Meier, Structure of a Complete ATP Synthase Dimer Reveals the Molecular Basis of Inner Mitochondrial Membrane Morphology, Mol. Cell. 63 (2016) 445–456. https://doi.org/10.1016/j.molcel.2016.05.037.

[6]   P.D. Boyer, Catalytic site occupancy during ATP synthase catalysis, FEBS Lett. 512 (2002) 29–32. https://doi.org/10.1016/S0014-5793(02)02293-7.

[7]   S. Nesci, F. Trombetti, V. Ventrella, A. Pagliarani, Opposite rotation directions in the synthesis and hydrolysis of ATP by the ATP synthase: hints from a subunit asymmetry, J. Membr. Biol. 248 (2015) 163–169. https://doi.org/10.1007/s00232-014-9760-y.

[8]   M. Strauss, G. Hofhaus, R.R. Schröder, W. Kühlbrandt, Dimer ribbons of ATP synthase shape the inner mitochondrial membrane, EMBO J. 27 (2008) 1154–1160. https://doi.org/10.1038/emboj.2008.35.

[9]   S. Nesci, A. Pagliarani, Incoming news on the F-type ATPase structure and functions in mammalian mitochondria, BBA Advances. 1 (2021) 100001. https://doi.org/10.1016/j.bbadva.2020.100001.

[10] G. Pinke, L. Zhou, L.A. Sazanov, Cryo-EM structure of the entire mammalian F-type ATP synthase, Nat Struct Mol Biol. 27 (2020) 1077–1085. https://doi.org/10.1038/s41594-020-0503-8.

[11] J. Karch, M.J. Bround, H. Khalil, M.A. Sargent, N. Latchman, N. Terada, P.M. Peixoto, J.D. Molkentin, Inhibition of mitochondrial permeability transition by deletion of the ANT family and CypD, Sci Adv. 5 (2019) eaaw4597. https://doi.org/10.1126/sciadv.aaw4597.

[12] M.A. Neginskaya, M.E. Solesio, E.V. Berezhnaya, G.F. Amodeo, N. Mnatsakanyan, E.A. Jonas, E.V. Pavlov, ATP Synthase C-Subunit-Deficient Mitochondria Have a Small Cyclosporine A-Sensitive Channel, but Lack the Permeability Transition Pore, Cell Rep. 26 (2019) 11-17.e2. https://doi.org/10.1016/j.celrep.2018.12.033.

[13] M.J. Hubbard, N.J. McHugh, Mitochondrial ATP synthase F1-beta-subunit is a calcium-binding protein, FEBS Lett. 391 (1996) 323–329.

[14] S. Nesci, F. Trombetti, V. Ventrella, M. Pirini, A. Pagliarani, Kinetic properties of the mitochondrial F1FO-ATPase activity elicited by Ca(2+) in replacement of Mg(2+), Biochimie. 140 (2017) 73–81. https://doi.org/10.1016/j.biochi.2017.06.013.

[15] V. Giorgio, V. Burchell, M. Schiavone, C. Bassot, G. Minervini, V. Petronilli, F. Argenton, M. Forte, S. Tosatto, G. Lippe, P. Bernardi, Ca(2+) binding to F-ATP synthase β subunit triggers the mitochondrial permeability transition, EMBO Rep. 18 (2017) 1065–1076. https://doi.org/10.15252/embr.201643354.

[16] N. Mnatsakanyan, E.A. Jonas, ATP synthase c-subunit ring as the channel of mitochondrial permeability transition: Regulator of metabolism in development and degeneration, J. Mol. Cell. Cardiol. 144 (2020) 109–118. https://doi.org/10.1016/j.yjmcc.2020.05.013.

[17] S. Nesci, A. Pagliarani, Ca2+ as cofactor of the mitochondrial H+-translocating F1FO-ATP(hydrol)ase, Proteins: Structure, Function, and Bioinformatics. 89 (2021) 477–482. https://doi.org/10.1002/prot.26040.

[18] T.M. Bauer, E. Murphy, Role of Mitochondrial Calcium and the Permeability Transition Pore in Regulating Cell Death, Circ Res. 126 (2020) 280–293. https://doi.org/10.1161/CIRCRESAHA.119.316306.

[19] S. Nesci, The mitochondrial permeability transition pore in cell death: A promising drug binding bioarchitecture, Medicinal Research Reviews. 40 (2020) 811–817. https://doi.org/10.1002/med.21635.

[20] G. Wang, Q. Peng, Y. Li, Lanthanide-Doped Nanocrystals: Synthesis, Optical-Magnetic Properties, and Applications, Accounts of Chemical Research. 44 (2011) 322–332. https://doi.org/10.1021/ar100129p.

[21] G. Strijkers, W. M. Mulder, G. F. van Tilborg, K. Nicolay, MRI Contrast Agents: Current Status and Future Perspectives, Anti-Cancer Agents in Medicinal Chemistry. 7 (2007) 291–305. https://doi.org/10.2174/187152007780618135.

[22] J. Chen, J. Ramos, M. Sirisawad, R. Miller, L. Naumovski, Motexafin gadolinium induces mitochondriallymediated caspase-dependent apoptosis, Apoptosis. 10 (2005) 1131–1142. https://doi.org/10.1007/s10495-005-0887-2.

[23] L. Pasquini, A. Napolitano, E. Visconti, D. Longo, A. Romano, P. Tomà, M.C.R. Espagnet, Gadolinium-Based Contrast Agent-Related Toxicities, CNS Drugs. 32 (2018) 229–240. https://doi.org/10.1007/s40263-018-0500-1.

11

[24] L.C. Adding, G.L. Bannenberg, L.E. Gustafsson, Basic Experimental Studies and Clinical Aspects of Gadolinium Salts and Chelates, Cardiovascular Drug Reviews. 19 (2006) 41–56. https://doi.org/10.1111/j.1527-3466.2001.tb00182.x.

[25] D.V. Bower, J.K. Richter, H. von Tengg-Kobligk, J.T. Heverhagen, V.M. Runge, Gadolinium-Based MRI Contrast Agents Induce Mitochondrial Toxicity and Cell Death in Human Neurons, and Toxicity Increases With Reduced Kinetic Stability of the Agent:, Investigative Radiology. 54 (2019) 453–463. https://doi.org/10.1097/RLI.0000000000000567.

[26] M.J. Akhtar, M. Ahamed, H. Alhadlaq, S. Alrokayan, Toxicity Mechanism of Gadolinium Oxide Nanoparticles and Gadolinium Ions in Human Breast Cancer Cells, Curr Drug Metab. 20 (2019) 907–917. https://doi.org/10.2174/1389200220666191105113754.

[27] J. Zhao, Z.-Q. Zhou, J.-C. Jin, L. Yuan, H. He, F.-L. Jiang, X.-G. Yang, J. Dai, Y. Liu, Mitochondrial dysfunction induced by different concentrations of gadolinium ion, Chemosphere. 100 (2014) 194–199. https://doi.org/10.1016/j.chemosphere.2013.11.031.

[28] S. Nesci, V. Ventrella, F. Trombetti, M. Pirini, A. Pagliarani, The mitochondrial F1FO-ATPase desensitization to oligomycin by tributyltin is due to thiol oxidation, Biochimie. 97 (2014) 128–137. https://doi.org/10.1016/j.biochi.2013.10.002.

[29] M.M. Bradford, A rapid and sensitive method for the quantitation of microgram quantities of protein utilizing the principle of protein-dye binding, Anal. Biochem. 72 (1976) 248–254. https://doi.org/10.1006/abio.1976.9999.

[30] C. Algieri, F. Trombetti, A. Pagliarani, V. Ventrella, C. Bernardini, M. Fabbri, M. Forni, S. Nesci, Mitochondrial Ca2+ -activated F1 FO -ATPase hydrolyzes ATP and promotes the permeability transition pore, Ann. N. Y. Acad. Sci. 1457 (2019) 142–157. https://doi.org/10.1111/nyas.14218.

[31] C. Algieri, F. Trombetti, A. Pagliarani, V. Ventrella, S. Nesci, Phenylglyoxal inhibition of the mitochondrial F1FO-ATPase activated by Mg2+ or by Ca2+ provides clues on the mitochondrial permeability transition pore, Arch. Biochem. Biophys. 681 (2020) 108258. https://doi.org/10.1016/j.abb.2020.108258.

[32] V. Ventrella, S. Nesci, F. Trombetti, P. Bandiera, M. Pirini, A.R. Borgatti, A. Pagliarani, Tributyltin inhibits the oligomycin-sensitive Mg-ATPase activity in Mytilus galloprovincialis digestive gland mitochondria, Comp. Biochem. Physiol. C Toxicol. Pharmacol. 153 (2011) 75–81. https://doi.org/10.1016/j.cbpc.2010.08.007.

[33] A. Cornish-Bowden, A simple graphical method for determining the inhibition constants of mixed, uncompetitive and non-competitive inhibitors, Biochem. J. 137 (1974) 143–144.

[34] V. Algieri, C. Algieri, L. Maiuolo, A. De Nino, A. Pagliarani, M.A. Tallarida, F. Trombetti, S. Nesci, 1,5-Disubstituted-1,2,3-triazoles as inhibitors of the mitochondrial Ca2+ -activated F1 FO -ATP(hydrol)ase and the permeability transition pore, Ann N Y Acad Sci. 1485 (2021) 43–55. https://doi.org/10.1111/nyas.14474.

[35] F. Ghanbari, K. Rowland-Yeo, J.C. Bloomer, S.E. Clarke, M.S. Lennard, G.T. Tucker, A. Rostami-Hodjegan, A critical evaluation of the experimental design of studies of mechanism based enzyme inhibition, with implications for in vitro-in vivo extrapolation, Curr Drug Metab. 7 (2006) 315–334. https://doi.org/10.2174/138920006776359293.

[36] S. Nesci, C. Algieri, F. Trombetti, V. Ventrella, M. Fabbri, A. Pagliarani, Sulfide affects the mitochondrial respiration, the Ca2+-activated F1FO-ATPase activity and the permeability transition pore but does not change the Mg2+-activated F1FO-ATPase activity in swine heart mitochondria, Pharmacol Res. 166 (2021) 105495. https://doi.org/10.1016/j.phrs.2021.105495.

[37] J.G. Graca, F.C. Davison, J.B. Feavel, Comparative toxicity of stable rare earth compounds. II. Effect of citrate and edetate complexing on acute toxicity in mice and guinea pigs, Arch Environ Health. 5 (1962) 437–444. https://doi.org/10.1080/00039896.1962.10663310.

[38] null Ermakov YuA, A.Z. Averbakh, A.B. Arbuzova, S.I. Sukharev, Lipid and cell membranes in the presence of gadolinium and other ions with high affinity to lipids. 2. A dipole component of the boundary potential on membranes with different surface charge, Membr Cell Biol. 12 (1998) 411–426.

[39] Y. Cheng, M. Liu, R. Li, C. Wang, C. Bai, K. Wang, Gadolinium induces domain and pore formation of human erythrocyte membrane: an atomic force microscopic study, Biochim Biophys Acta. 1421 (1999) 249–260. https://doi.org/10.1016/s0005-2736(99)00125-x.

[40] E.C. Gianulis, A.G. Pakhomov, Gadolinium modifies the cell membrane to inhibit permeabilization by nanosecond electric pulses, Arch Biochem Biophys. 570 (2015) 1–7. https://doi.org/10.1016/j.abb.2015.02.013.

[41] I.H. Segel, Enzyme Kinetics, in: W.J. Lennarz, M.D. Lane (Eds.), Encyclopedia of Biological Chemistry, Academic Press, Waltham, 2013: pp. 216–220. https://doi.org/10.1016/B978-0-12-378630-2.00012-8.

[42] R. Casadio, B.A. Melandri, CaATP inhibition of the MgATP-dependent proton pump (H+-ATPase) in bacterial photosynthetic membranes with a mechanism of alternative substrate inhibition, JBIC. 1 (1996) 284–291. https://doi.org/10.1007/s007750050055.

[43] W.D. Frasch, The participation of metals in the mechanism of the F(1)-ATPase, Biochim. Biophys. Acta. 1458 (2000) 310–325.

[44] L. Nathanson, Z. Gromet-Elhanan, Mutations in the β-subunit Thr159 and Glu184 of the Rhodospirillum rubrum F0F1 ATP synthase reveal differences in ligands for the coupled Mg2+- and decoupled Ca2+-dependent F0F1 activities, Journal of Biological Chemistry. 275 (2000) 901–905. https://doi.org/10.1074/jbc.275.2.901.

[45] H. Liu, L. Yuan, X. Yang, K. Wang, La(3+), Gd(3+) and Yb(3+) induced changes in mitochondrial structure, membrane permeability, cytochrome c release and intracellular ROS level, Chem Biol Interact. 146 (2003) 27–37. https://doi.org/10.1016/s0009-2797(03)00072-3.

[46] X. Feng, Q. Xia, L. Yuan, X. Yang, K. Wang, Impaired mitochondrial function and oxidative stress in rat cortical neurons: implications for gadolinium-induced neurotoxicity, Neurotoxicology. 31 (2010) 391–398. https://doi.org/10.1016/j.neuro.2010.04.003.

[47] J. Zhao, L. Ma, X. Xiang, Q.-L. Guo, F.-L. Jiang, Y. Liu, Microcalorimetric studies on the energy release of isolated rat mitochondria under different concentrations of gadolinium (III), Chemosphere. 153 (2016) 414–418. https://doi.org/10.1016/j.chemosphere.2016.03.082.

[48] W.-H. Zhang, J.-S. Wang, Y. Zhou, J.-Y. Li, Gadolinium chloride and salvia miltiorrhiza compound ameliorate reperfusion injury in hepatocellular mitochondria, World J Gastroenterol. 9 (2003) 2040–2044. https://doi.org/10.3748/wjg.v9.i9.2040.

[49] M. Chen, Y. Zheng, Y. Song, J. Xue, Z. Liang, X. Yan, D. Luo, Pretreatment with low-dose gadolinium chloride attenuates myocardial ischemia/reperfusion injury in rats, Acta Pharmacol Sin. 37 (2016) 453–462. https://doi.org/10.1038/aps.2015.156.

[50] T. Yu, M. Zhen, J. Li, Y. Zhou, H. Ma, W. Jia, C. Wang, Anti-apoptosis effect of amino acid modified gadofullerene via a mitochondria mediated pathway, Dalton Trans. 48 (2019) 7884–7890. https://doi.org/10.1039/c9dt00800d.

Figure captions

Figure 1. Subunit composition of mammalian mitochondrial F_1F_O-ATPase. The enzyme subunits are drawn as ribbon representations obtained from modified PDB ID code: 6TT7. The letter colors are the same as those of the subunits to which the structures belong.

Figure 2. Dose-response curve of $GdCl_3$ inhibition of the F_1F_O-ATPase activity. A) F_1F_O-ATPase activated by Mg^{2+} (Mg^{2+}-activated F_1F_O-ATPase) (□) and by Ca^{2+} (Ca^{2+}-activated F_1F_O-ATPase) (○) activities in the presence of increasing $GdCl_3$ concentrations. Data represent the mean ± SD from three independent experiments carried out on different mitochondrial preparations.

13

Figure 3. Inhibition kinetics of the mitochondrial Mg^{2+}-activated F_1F_O-ATPase by $GdCl_3$. Dixon (A, C) and Cornish–Bowden (B, D) plots at 2mM $MgCl_2$ plus 3 mM (○) or 6 mM (●) ATP (A,B); at 6 mM ATP plus 0.5 mM (□) or 2 mM (■) Mg^{2+} (C, D). The experimental design to build these plots is detailed in Section 2.4. All points represent the mean ± SD (vertical bars) of four distinct experiments carried out on different mitochondrial preparations.

Figure 4. Inhibition kinetics of the mitochondrial Ca^{2+}-activated F_1F_O-ATPase by $GdCl_3$. Dixon (A, C) and Cornish–Bowden (B, D) plots at 2mM $CaCl_2$ plus 1 mM (○) or 3 mM (●) ATP (A,B); at 3 mM ATP plus 0.5 mM (□) or 2 mM (■) Ca^{2+} (C, D) The experimental design to build these plots is detailed in Section 2.4. All points represent the mean ± SD (vertical bars) of four distinct experiments carried out on different mitochondrial preparations.

Figure 5. Inactivation kinetics of the Mg^{2+}-activated F_1F_O-ATPase by increasing $GdCl_3$ concentrations. (A) Semilogarithmic plot of the residual activity (Θ) *versus* time at fixed concentrations of $GdCl_3$ (Δ) 1.0 mM, (◊) 2.0 mM, (□) 4.0 mM. (B) Replot of the reciprocal of first-order rate constant (k_{obs}) from the straight lines of (A). Each point corresponds to $GdCl_3$ (▲) 1.0 mM, (♦) 2.0 mM, and (■) 4.0 mM. The experimental design to build these plots is detailed in Section 2.4. All points represent the mean ± SD (vertical bars) of four distinct experiments carried out on different mitochondrial preparations.

Figure 6. Inactivation kinetics of the Ca^{2+}-activated F_1F_O-ATPase by increasing $GdCl_3$ concentrations. (A) Semilogarithmic plot of the residual activity (Θ) *versus* time at fixed concentrations of $GdCl_3$ (○) 1.0 mM, (□) 1.5 mM, (□) 2.0 mM. (B) Replot of the reciprocal of first-order rate constant (k_{obs}) from the straight lines of (A). Each point corresponds to 1.0 mM $GdCl_3$ (●) 1.5 mM $GdCl_3$ (■) and 2 mM (▲). The experiments were carried out as detailed in Section 2.4. All points represent the mean ± SD (vertical bars) of four distinct experiments carried out on different mitochondrial preparations.

Figure 7. Evaluation of mPTP opening. Representative curves (A) of the calcium retention capacity (CRC). CRC was monitored in response to subsequent 10 µM $CaCl_2$ pulses (shown by the arrows), as detailed in the Section 2.5, in the absence (Control-black line) and in the presence of the inhibitors 2 mM MgADP (red line), and 1 mM $GdCl_3$ (green line). B) Quantitation of the mPTP displayed as the ratio of the number of calcium pulses required to induce the mPTP opening in MgADP-inhibited (CRC_i) and uninhibited (CRC_o) mitochondria. Data represent the mean ± SD from three independent experiments carried out on distinct mitochondrial preparations. * indicates significant differences with respect to the control ($P \leq 0.05$).
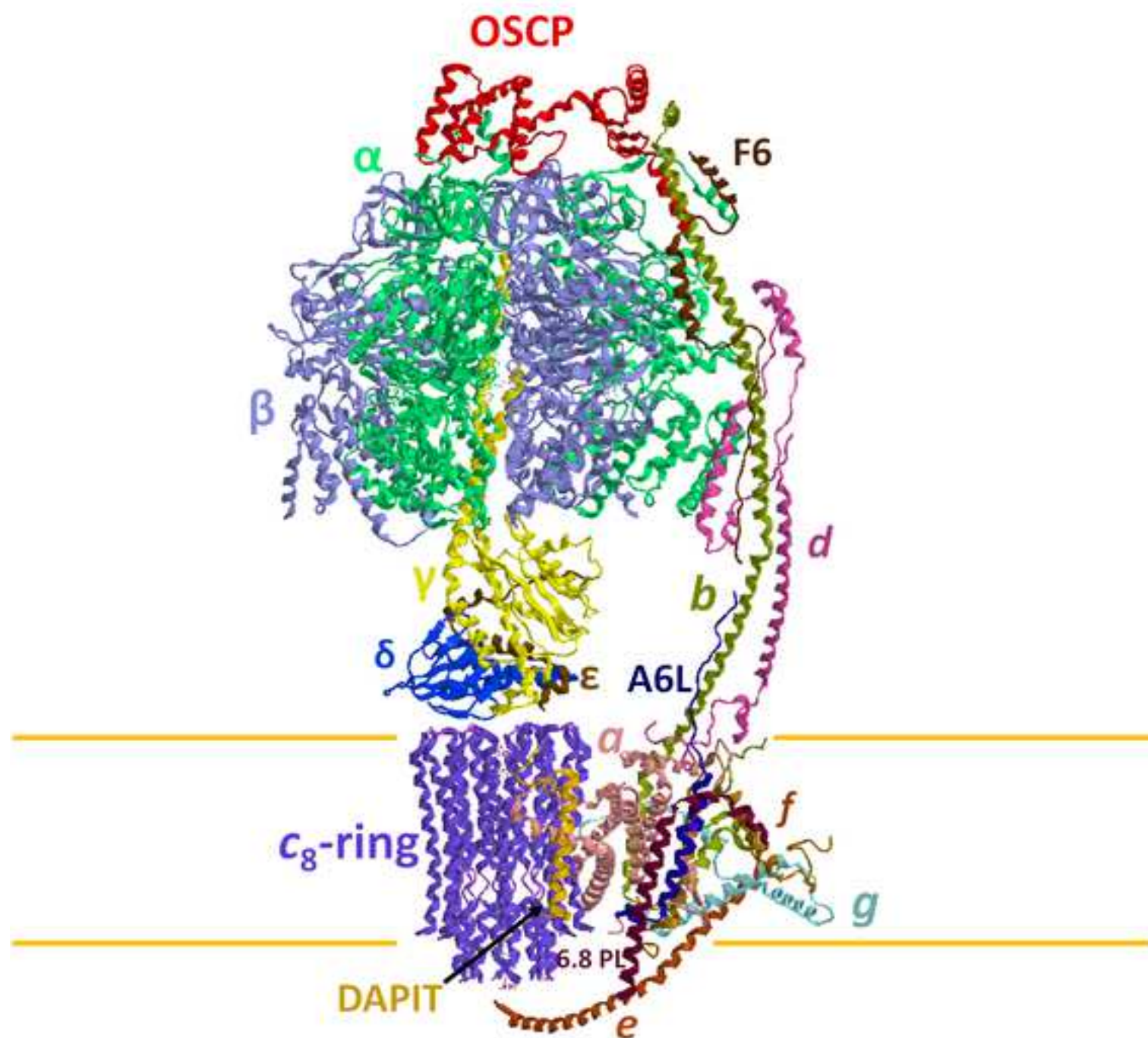
14

Figure 1

Figure 2

A)

B)
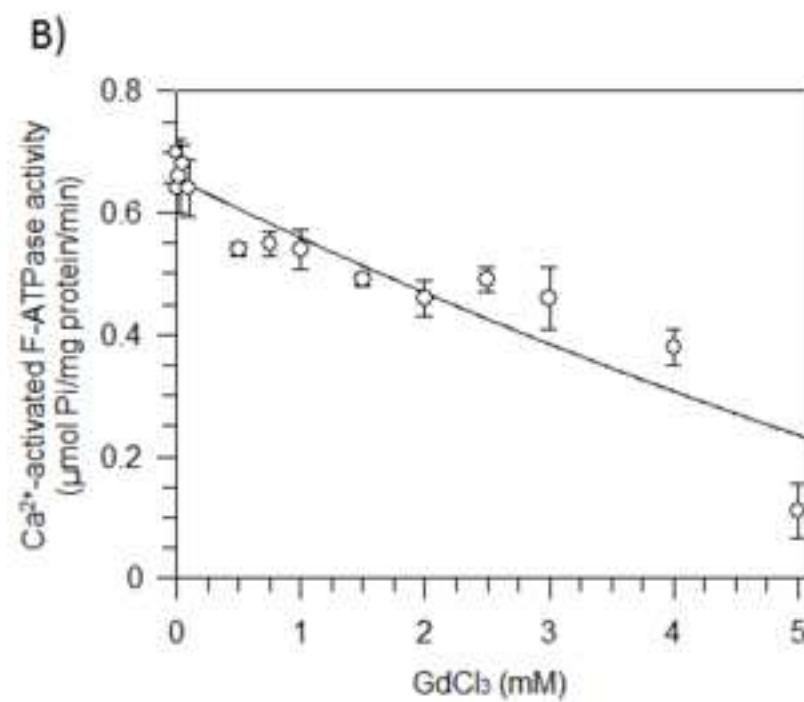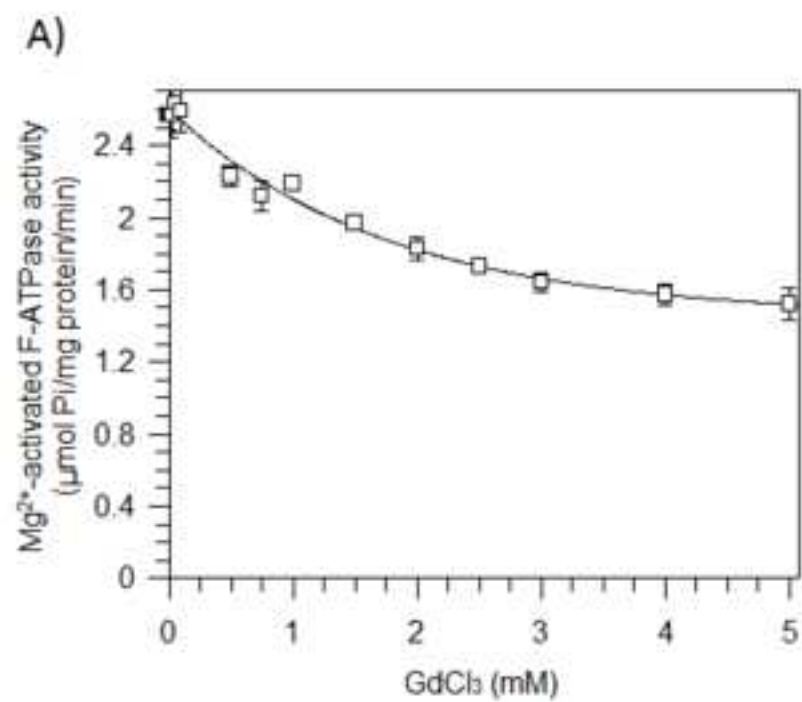
Figure 3   Click here to access/download;Figure;Figure 3.tif ⬦

Figure 4
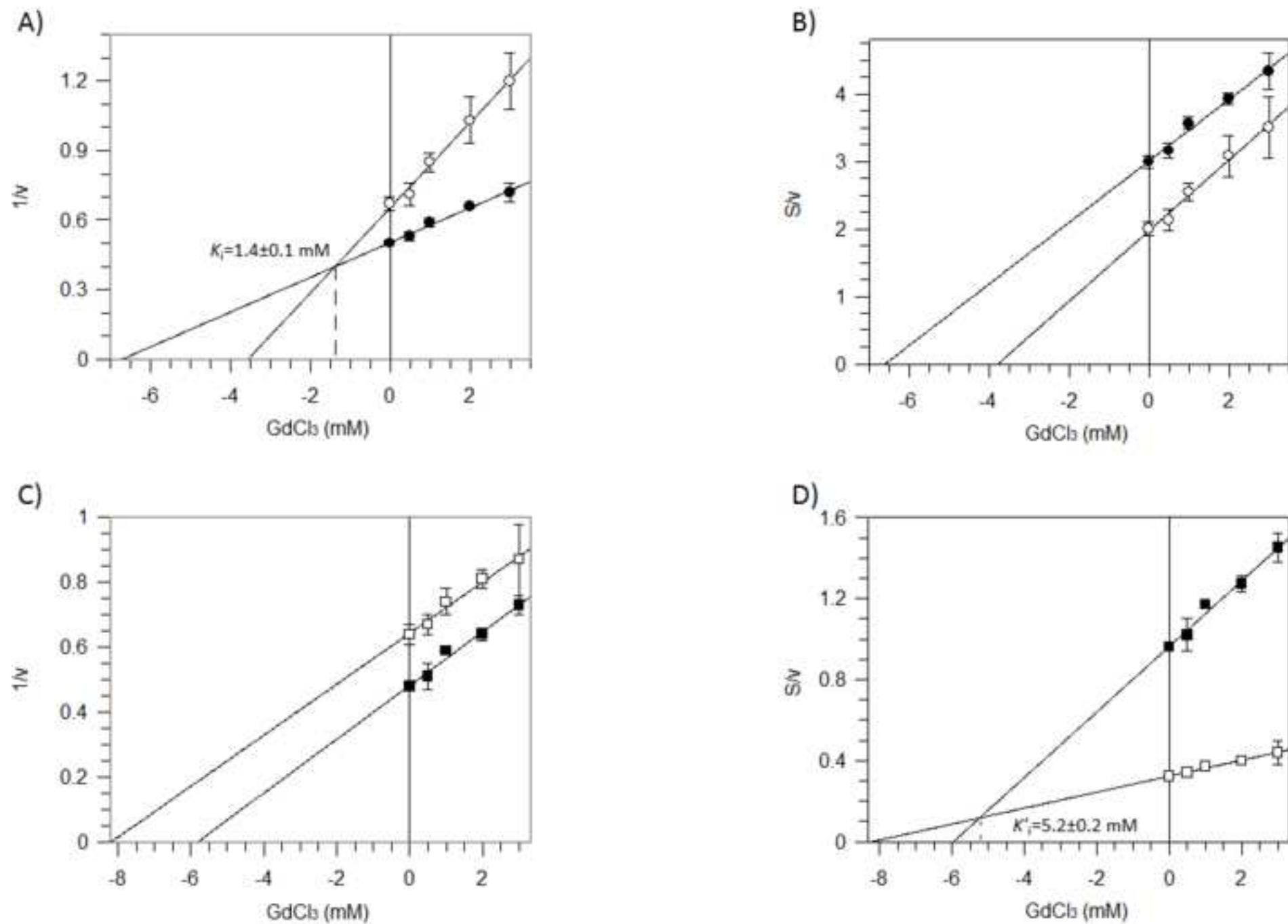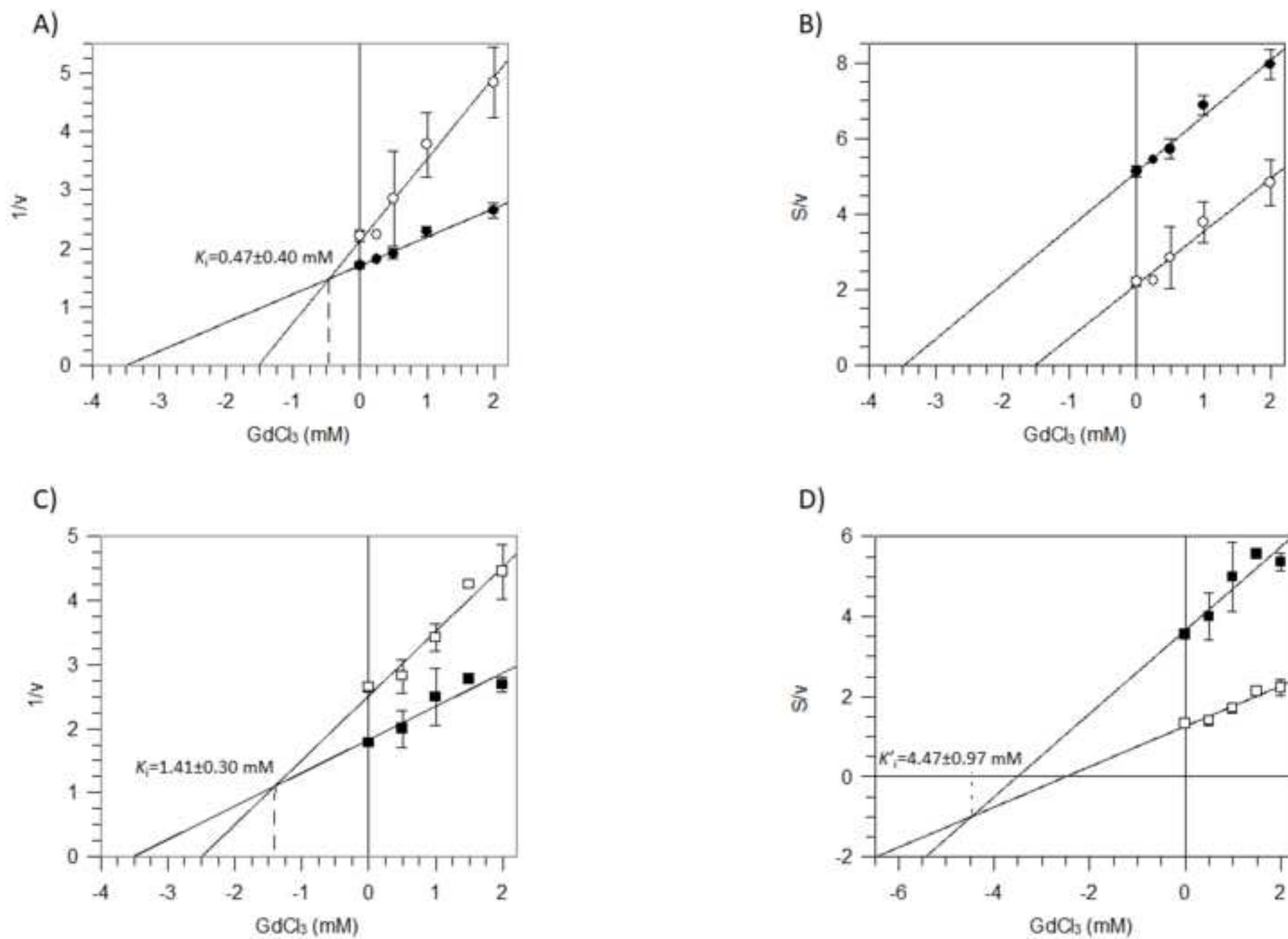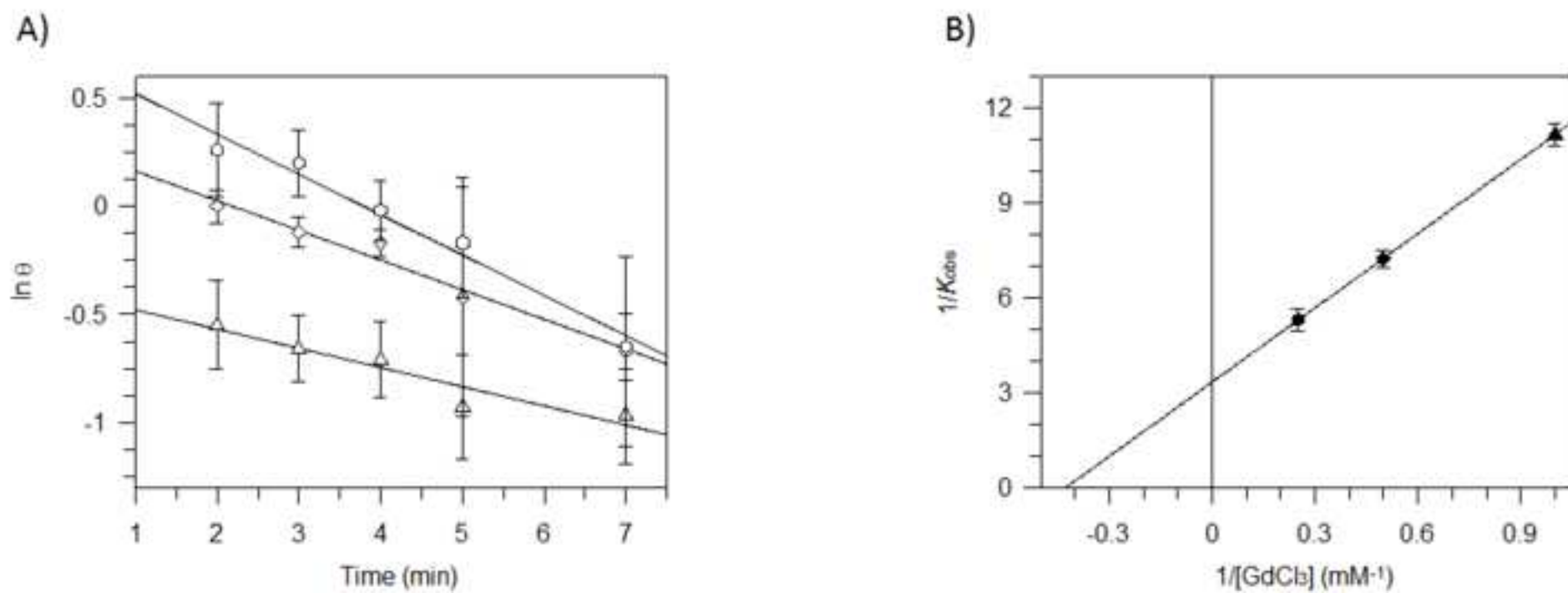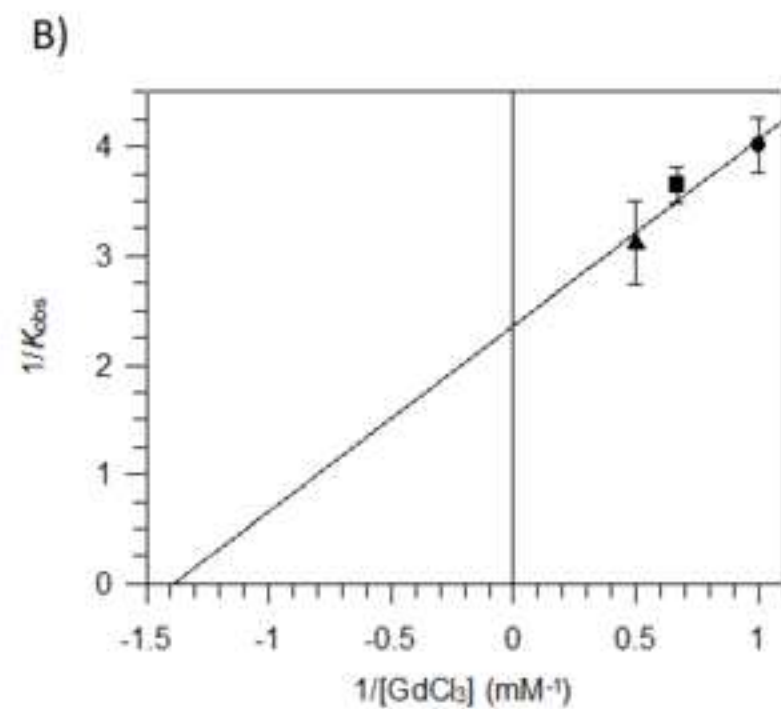
Click here to access/download;Figure;Figure 4.tif

A)

$K_i = 0.47 \pm 0.40$ mM

C)

$K_i = 1.41 \pm 0.30$ mM

D)

$K'_i = 4.47 \pm 0.97$ mM

Figure 5

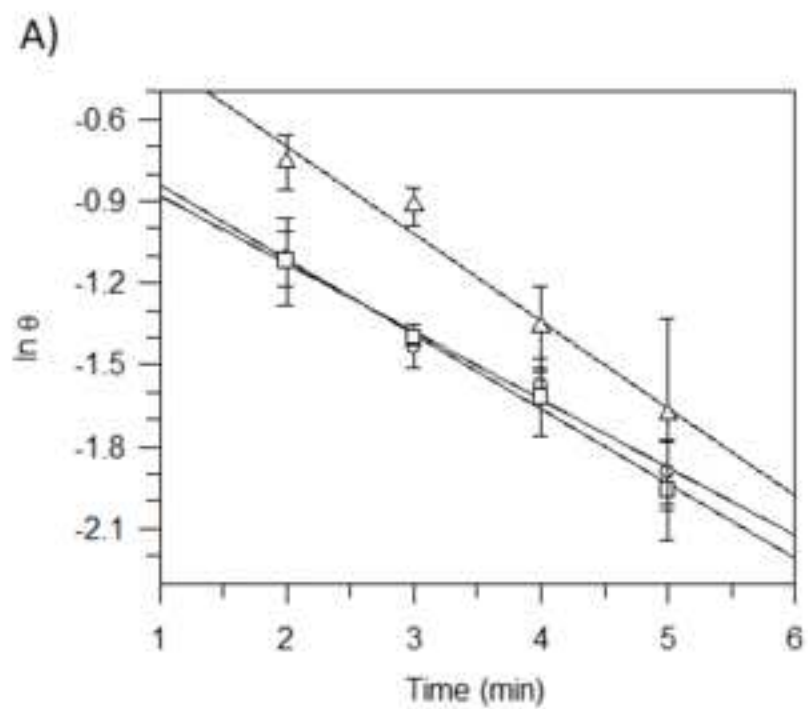Click here to access/download;Figure;Figure 5.tif ⬇
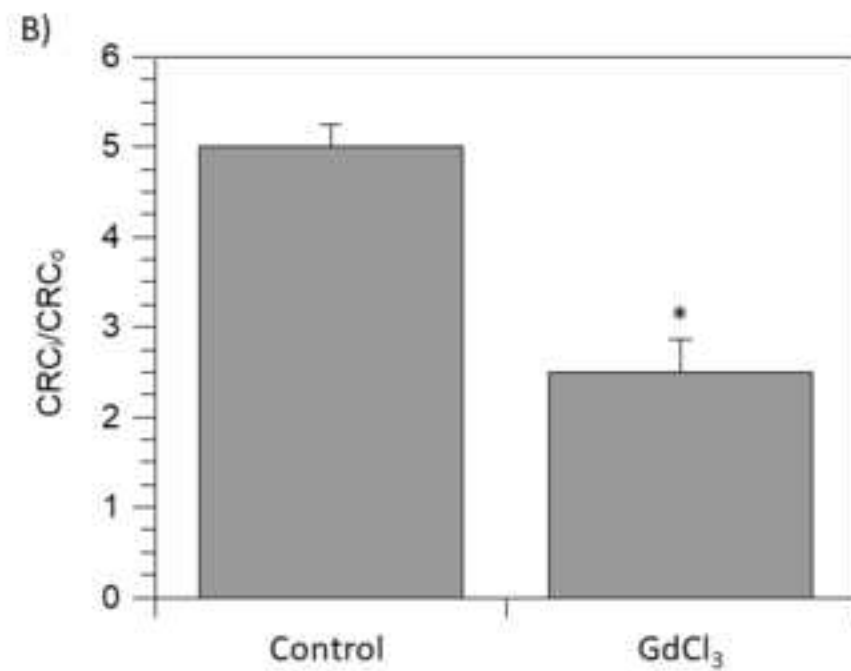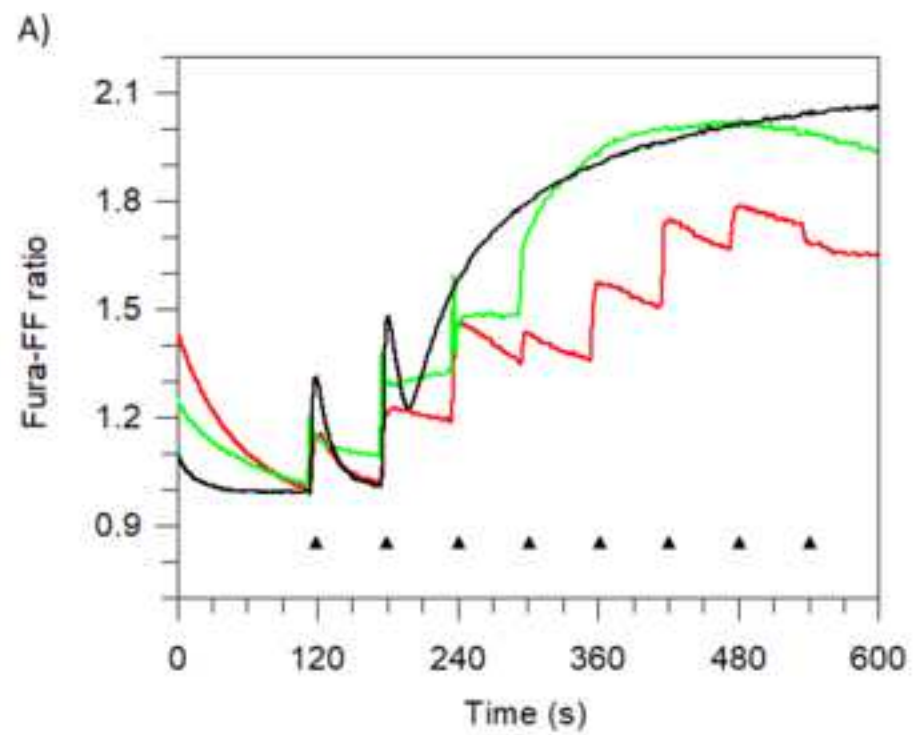
Figure 6

Figure 7

A)

B)

Table 1

Kinetic constants of Gd^{3+} inhibition on the F_1F_O-ATPase activated by the cofactors Mg^{2+} or Ca^{2+}.

	ATP substrate		Cofactor		K_I (mM)	k_{inact} (s^{-1})	k_{inact}/K_I (mM$^{-1}\cdot$s^{-1})
	K_i (mM)	K'_i (mM)	K_i (mM)	K'_i (mM)			
Mg^{2+}-ATPase	1.4±0.1A	∞	∞	5.2±0.2A	2.35±0.35A	0.30±0.04A	0.13±0.02A
Ca^{2+}-ATPase	0.5±0.4B	∞	1.4±0.3a	4.5±1.0Ab	0.72±0.11B	0.42±0.06B	0.59±0.09B

F_1F_O-ATPase activated by Mg^{2+} (Mg^{2+}-ATPase); F_1F_O-ATPase activated by Ca^{2+} (Ca^{2+}-ATPase); Substrate (ATP); Cofactor (Mg^{2+} or Ca^{2+}). K_i and K'_i values were graphically obtained from the Dixon and Cornish Bowden plots, respectively reported in Fig. 3 for Mg^{2+}-activated F_1F_O-ATPase and in Fig. 5 for the Ca^{2+}-activated F_1F_O-ATPase. K_I and k_{inact} values of Mg^{2+}-activated F_1F_O-ATPase or Ca^{2+}-activated F_1F_O-ATPase were graphically obtained from the double reciprocal plots of Fig. 4B and Fig. 5B, respectively. Details are reported in the section 2.4. Data are the mean ± SD of three different experiments carried out on distinct mitochondrial pools. Different upper case letters indicate significantly different values ($P\leq0.05$) between different activated F_1F_O-ATPases; different lower case letters indicate different values ($P\leq0.05$) within the same treatment. ∞= not detectable.

Abbreviations

Author Statement

CA, investigation and methodology;FT and AP, writing - review & editing; MF, resources; AP and SN, visualization; FT, AP and SN, validation; SN, supervision and writing origina draft.